Neandertal roots: Cranial and chronological evidence from Sima de los Huesos

J. L. Arsuaga *et al.*

Science **344**, 1358 (2014);
DOI: 10.1126/science.1253958

Science (print ISSN 0036-8075; online ISSN 1095-9203) is published weekly, except the last week in December, by the American Association for the Advancement of Science, 1200 New York Avenue NW, Washington, DC 20005.

RESEARCH ARTICLE

HUMAN EVOLUTION

Neandertal roots: Cranial and chronological evidence from Sima de los Huesos

J. L. Arsuaga,[1,2]* I. Martínez,[3,1] L. J. Arnold,[4,5] A. Aranburu,[6] A. Gracia-Téllez,[3,1] W. D. Sharp,[7] R. M. Quam,[8,9,1] C. Falguères,[10] A. Pantoja-Pérez,[1,2] J. Bischoff,[11] E. Poza-Rey,[1,2] J. M. Parés,[4] J. M. Carretero,[12] M. Demuro,[4,13] C. Lorenzo,[14,15,1] N. Sala,[1] M. Martinón-Torres,[4] N. García,[1,2] A. Alcázar de Velasco,[1] G. Cuenca-Bescós,[16] A. Gómez-Olivencia,[1,10,17] D. Moreno,[10,12] A. Pablos,[1,4,12] C.-C. Shen,[18] L. Rodríguez,[12] A. I. Ortega,[4] R. García,[12] A. Bonmatí,[1,2] J. M. Bermúdez de Castro,[4] E. Carbonell[15,14,19]

Seventeen Middle Pleistocene crania from the Sima de los Huesos site (Atapuerca, Spain) are analyzed, including seven new specimens. This sample makes it possible to thoroughly characterize a Middle Pleistocene hominin paleodeme and to address hypotheses about the origin and evolution of the Neandertals. Using a variety of techniques, the hominin-bearing layer could be reassigned to a period around 430,000 years ago. The sample shows a consistent morphological pattern with derived Neandertal features present in the face and anterior vault, many of which are related to the masticatory apparatus. This suggests that facial modification was the first step in the evolution of the Neandertal lineage, pointing to a mosaic pattern of evolution, with different anatomical and functional modules evolving at different rates.

The course of human evolution in the Middle Pleistocene is controversial (*1*–*4*). Most of the debate has focused on taxonomic and phylogenetic questions, particularly surrounding the origin of Neandertals and modern humans (*5*–*9*). The European Middle Pleistocene fossil record is important for the timing and pattern of emergence of the Neandertals, but it is composed mainly of isolated and geographically dispersed remains of diverse chronologies. This complicates the evaluation of competing evolutionary scenarios. One of these scenarios, known as the "accretion model," rests on two hypotheses: one regarding the timing of the origin of the Neandertal lineage and the other regarding the pattern of morphological change (*1*, *5*, *10*). Under this model, the Neandertals would have deep roots in the Middle Pleistocene, branching off as early as Marine Isotope Stage 11 [around 400,000 years ago (400 ka)] (*5*, *11*), or even earlier. In addition, the model suggests that the full suite of derived Neandertal features (anatomical and functional modules) did not emerge as a single package, but that different features appeared separately and at different times. In particular, Neandertal facial morphology evolved first, followed by changes in the neurocranium.

Here we analyze a collection of 17 well-dated skulls, including several previously unpublished specimens [Fig. 1, supplementary text S1 (*12*), and table S1], that can be used to test the two pillars of the accretion model. This sample comes from the Sima de los Huesos (SH) Middle Pleistocene site in the Sierra de Atapuerca (Spain) and derives from a single paleo-deme (p-deme). Because the accretion model is based mainly on nonmetric traits (*5*), our analysis emphasizes the pattern of expression of morphological features in the SH hominins, although the descriptive statistics for the principal craniometrical variables in the SH sample are also provided (table S2).

A new age for SH hominins

The SH site is a small chamber at the foot of a shaft located deep inside an underground karst

Fig. 1. Cranium 9 (top left), Cranium 15 (top right), and Cranium 17 (bottom) from SH. Scale bar: 3 cm.

[1]Centro Mixto UCM-ISCIII de Evolución y Comportamiento Humanos, Madrid, Spain. [2]Departamento de Paleontología, Facultad Ciencias Geológicas, Universidad Complutense de Madrid, Spain. [3]Área de Paleontología, Departamento de Geología, Geografía y Medio Ambiente, Universidad de Alcalá, Spain. [4]Centro Nacional de Investigación sobre la Evolución Humana Burgos, Spain. [5]School of Earth and Environmental Sciences, the Environment Institute, and the Institute for Photonics and Advanced Sensing (IPAS), University of Adelaide, Australia. [6]Departamento Mineralogía y Petrología, Facultad de Ciencia y Tecnología, Universidad del País Vasco, Spain. [7]Berkeley Geochronology Center, Berkeley, CA, USA. [8]Department of Anthropology, Binghamton University (State University of New York), Binghamton, NY, USA. [9]Division of Anthropology, American Museum of Natural History, New York, NY, USA. [10]Département de Préhistoire, Muséum National d'Histoire Naturelle, Paris, France. [11]U.S. Geological Survey, Menlo Park, CA, USA. [12]Laboratorio de Evolución Humana, Departamento de Ciencias Históricas y Geografía, Universidad de Burgos, Spain. [13]Institute for Photonics and Advanced Sensing (IPAS), School of Chemistry and Physics, University of Adelaide, Australia. [14]Àrea de Prehistòria, Departamento d'Història i Història de l'Art, Universitat Rovira i Virgili (URV), Tarragona, Spain. [15]Institut Català de Paleoecologia Humana i Evolució Social, Tarragona, Spain. [16]Paleontología, Aragosaurus-IUCA and Facultad Ciencias, Universidad de Zaragoza, Spain. [17]PAVE Research Group, Division of Biological Anthropology, Cambridge, UK. [18]High-Precision Mass Spectrometry and Environment Change Laboratory (HISPEC), Department of Geosciences, National Taiwan University, Taiwan ROC. [19]Institute of Vertebrate Paleontology and Paleoanthropology of Beijing (IVPP), China.
***Corresponding author. E-mail: jlarsuaga@isciii.es**

system (*13*). To date, more than 6500 human fossils from at least 28 individuals are represented in a single stratigraphic level that we have redated using a suite of numerical and relative dating methods (*12*).

The SH sedimentary record can be subdivided into 12 lithostratigraphic units (LU-1 to LU-12) (supplementary text S2). Of these, only LU-6 and LU-7 contain hominin and carnivore remains (Fig. 2). LU-6 consists of plastic red-brown clays with a high density of hominin and carnivore fossils and varying amounts of speleothem intraclasts. U-series dating of a cave raft speleothem deposited directly on a hominin cranium (cranium 4) from LU-6 yielded a mean age of 434 +36/–24 ka (n = 5; supplementary text S3 and S4). We interpret this age to be pene-contemporaneous with the deposition of the cranium. The new age is consistent with the early-Middle to mid-Middle Pleistocene age for the faunal assemblage of LU-6 and LU-7 (supplementary text S5). New paleomagnetic samples collected from four stratigraphic exposures yielded exclusively normal polarities for LU-6 (n = 28; supplementary text S6), consistent with previous paleomagnetic interpretations that the hominin bones accumulated during the Brunhes chron (<780 ka) (*14*). Combined electron spin resonance/uranium-series (ESR/U-series) analysis of a bear tooth from LU-6 provided an age of 261 +26/–25 ka, which is interpreted as a minimum age owing to uncertainties with the geochemical and dosimetry histories of this specimen (supplementary text S7).

The overlying sediments (LU-7) were transported into SH as a debris flow that incorporated large-carnivore bones, mainly those of bears previously accumulated in the Ramp section of the site, and locally eroded and incorporated some hominin and bear fossils from LU-6. The magnetic polarity of LU-7 is normal and consistent with a Brunhes depositional age (n = 9; supplementary text S6). All six of the TT-OSL and pIR-IR ages (428 ± 27 to 441 ± 25 ka for K-feldspar and 396 ± 35 to 429 ± 32 ka for quartz; supplementary text S8) and one of the ESR quartz ages (443 ± 90 ka; supplementary text S7) for this unit are statistically indistinguishable and support sedimentological evidence for a short-lived depositional episode. Although two additional ESR quartz samples taken from LU-7 yielded significantly older ages of 0.9 to 1.5 Ma, these are interpreted as maximum ages owing to potential methodological complications.

Cranial capacities and encephalization quotient (EQ)

The cranial capacity can only be measured directly in crania (Cr.) 4, 5, and 6 (*15*, *16*). Twelve other crania in the SH collection are sufficiently well preserved to allow for a good estimation of the cranial capacity on the basis of endocast scaling (Fig. 3 and supplementary text S9). The mean of the SH cranial capacities (1232 cm^3; n = 15, table S3) is clearly above the Asian *Homo erectus* mean. It is also well below the Neandertal and Pleistocene *H. sapiens* means and similar to the mean of the non–*H. erectus* Middle Pleistocene sample (fig. S1). The mean EQ obtained for the SH hominins (3.27) is lower

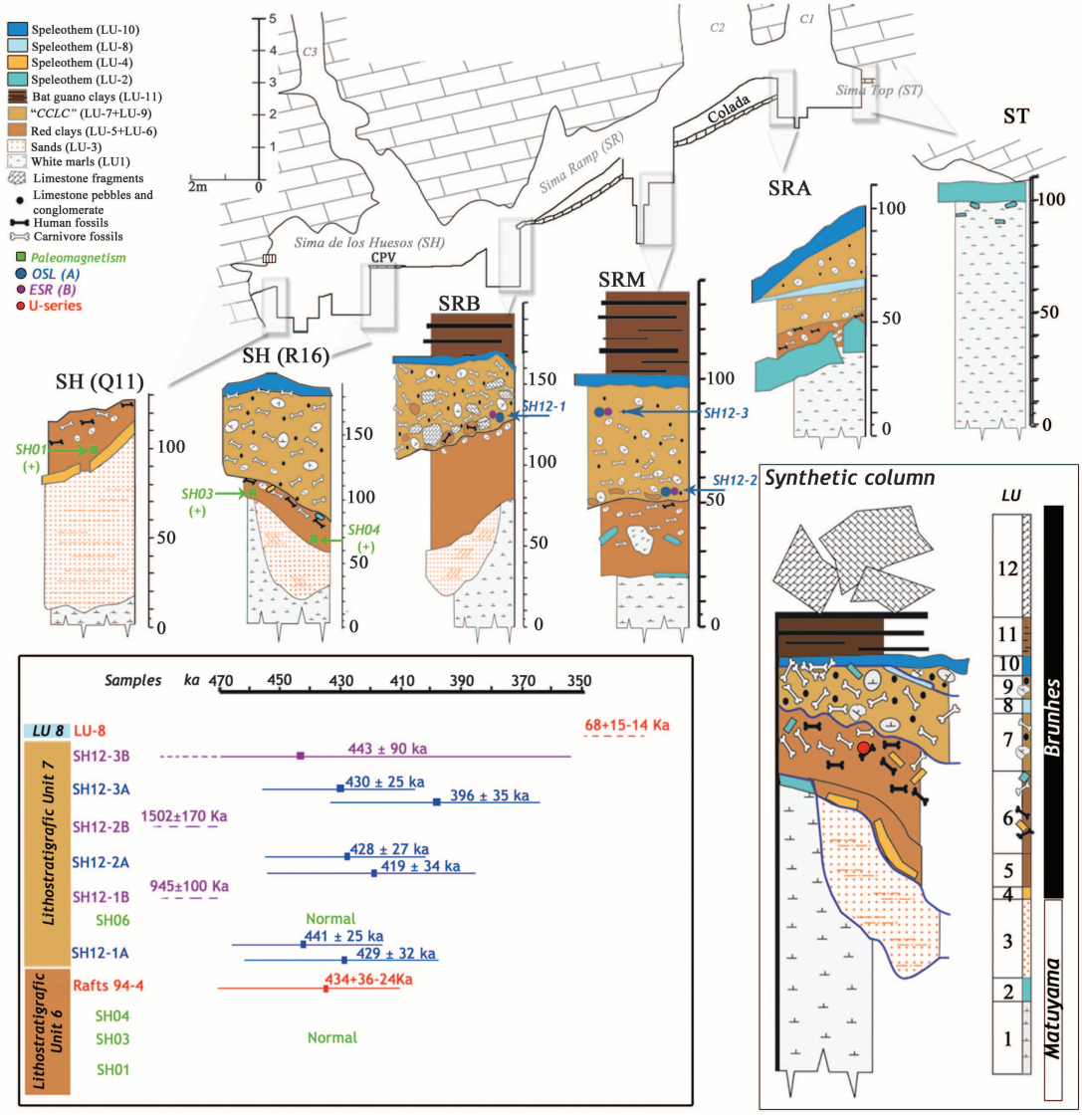

Fig. 2. Cross-section of SH showing the different stratigraphic columns exposed throughout the site. The composite stratigraphic section is shown, as are the sampling positions and ages obtained. The colors used correspond to those of the Munsell color for wet sediment. The inferred geomagnetic polarity zones are based on the results presented in this study for LU-5 to LU-7, and results for LU-2 to LU-10 were presented in (*14*, *45*).

than in modern humans and Neandertals (tables S4 and S5).

Cranial regions (Table 1)

Cranial vault

In the SH crania, the opisthocranion lies on the occipital plane, but the difference with the cranial length taken on the occipital torus is small. In contrast, in early *Homo* and Asian *H. erectus*, the opisthocranion always falls on the occipital torus. This same condition can be found at Ceprano. In *H. sapiens* and Neandertals, the opisthocranion lies clearly on the occipital plane of the occipital bone, well above the superior nuchal line. Although the SH occipital plane exhibits a certain degree of curvature, it is considerably less curved than in Neandertals, and there is no occipital bun ("chignon").

The temporal squama outline is consistently very convex in the SH sample, with an arched or subtriangular superior border, as seen in African and European Middle Pleistocene hominins (MPHs), Neandertals, and *H. sapiens*. The angular torus is absent in most SH specimens, although there are hints of it in some cases (Cr. 2, 5, 7), and it is more clearly expressed in Cr. 4. Arago and Ceprano are the only other European MPHs that clearly show this structure.

The maximum cranial breadth consistently lies in a low position, but the lateral cranial walls are either parallel or slightly convergent superiorly. This condition is similar to other European MPHs (Swanscombe, Steinheim, Reilingen, Petralona) and departs from the primitive state of convergent lateral walls of the braincase in early *Homo* and Asian *H. erectus* (*17*, *18*). It is also different from the derived conditions seen in Neandertals (circular outline) and most *H. sapiens* (divergent lateral walls with marked parietal bosses) (*19*–*21*).

The occipital torus of the SH specimens is generally weak, and mainly developed in the central region of the occipital squama, fading out toward the asterion. The tori are straight, do not have depressions in the middle, and are not bilaterally projecting, in contrast to Neandertals. Above the torus there is always a large central semicircular area, which is flat or even slightly convex and shows a concentration of small circular excavations. This pattern is attenuated, however, in Cr. 1, 4, and 5 (all mature adults). The flat, central, and semicircular supratoral area is clearly distinguishable from the rest of the occipital plane, and the opisthocranion lies precisely on its superior limit. A similar suprainiac morphology can be found in the Swanscombe sample. However, this individual shows more of a depression and the occipital torus is bilaterally projecting, as in Steinheim and Neandertals. Although the "cratered" surface of the SH specimens could be interpreted as reminiscent of the Neandertal suprainiac fossa (*16*, *19*), the latter is smaller, clearly sunken, and more inferiorly oriented. The SH condition is also different from that of the Vertëszöllos sample, which exhibits a high and slightly inflated occipital "torus" without a flat or depressed suprainiac area (*20*).

Most of the SH crania show a supraorbital torus that is double-arched and rounded (smoothly rolled) in a parasagittal section (though Cr. 13 shows a slight "torsion" between the glabellar segment and the more lateral parts of the ridge). There is no division of the torus into separate arches, although a shallow depression can be seen occasionally in the glabellar region (e.g., Cr. 13). The general SH pattern closely approaches the derived Neandertal morphology of the supraorbital torus and is clearly different from that of Arago, Kabwe, and Ceprano (being closer to Petralona).

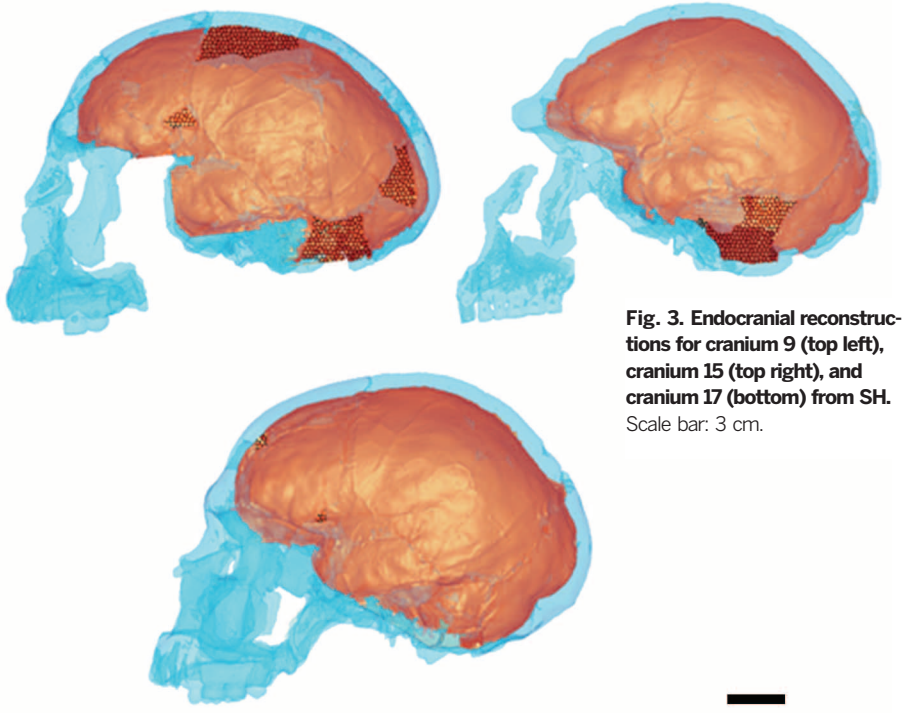

Fig. 3. Endocranial reconstructions for cranium 9 (top left), cranium 15 (top right), and cranium 17 (bottom) from SH. Scale bar: 3 cm.

Facial skeleton

The inferior malar border in the SH sample is gently arched, and the zygomatic root is located midway between the low (Neandertal) and the high (modern human) placements. The nasal root projects sagittally to the same degree as glabella (i.e., it is not depressed), and the nasal bones are horizontally oriented. In addition, the nasal spine is placed in a forward position in the SH specimens, with zygomaxillary angles within the Neandertal range of variation (fig. S10). There is some maxillary flexion, so that the infraorbital plate and the lateral wall of the nasal cavity do not form the same plane. Thus, there is an advanced degree of midfacial prognathism in the SH midface, but it is not as inflated, smooth, and retreating as in Neandertals.

Unlike the nasal morphology of Neandertals (*22*), a raised rim of the internal nasal margin is not formed in any SH cranium, and the transition between the clivus and the nasal cavity floor is smooth. The lateral nasal crest fades out in the nasoalveolar clivus at the level of the I^2, without merging with the spinal crest or reaching the nasal spine. Moreover, as has been noted by others (*23*), the "medial projection" [a wide, broad-base mass in the nasal wall that protrudes medially into the nasal cavity (*22*)] typical of the Neandertals is not seen in the SH sample. Finally, the nasal floor of the SH specimens is level or sloped and never sunken or bilevel, as is found in many Neandertals (*24*).

The dental arcade of the SH hominins generally shows approximately parallel postcanine toothrows and a frontal alignment of the anterior dentition, resulting in a fairly square outline. A more exaggerated expression of this dental arcade shape can be seen in Petralona and is also variably present in Neandertals.

Basicranium

The mastoid processes are more projecting than the weakly developed juxtamastoid eminence, particularly in the adult individuals, and no anterior mastoid tubercle is present in the SH sample. For these three features, the SH sample displays primitive morphology and contrasts with the derived Neandertal condition (*10*, *21*). The tympanic plate is coronally oriented in nearly all the SH specimens, which is a primitive condition also seen in Neandertals. The styloid process is fused to the basicranium, which is the primitive character state for the genus *Homo*, with Asian *H. erectus* showing a derived (non-fused) styloid process (*25*). Unlike in Neandertals (*26*), the styloid process is aligned with the stylomastoid foramen and the digastric groove in the SH sample.

A large postglenoid process is characteristic of Neandertals (*27*) and European MPHs (e.g., Steinheim, Bilzingsleben G1), but in the SH crania it is even more developed. In contrast, the articular

Table 1. Morphological traits in SH crania. See figs. S2 to S9 for illustration of the traits on the SH cranial sample and table S6 for the individual scores.

Trait	State
Occipital torus shape	Straight in inferior and posterior views: *N* = 9
Occipital torus extension	Fading toward the asterion: *N* = 8 Extends to the asterion: *N* = 2 (Cr. 1, Cr.4)
Oval-shaped area of dense "cratered" surface placed above the occipital torus	Present: *N* = 10
Maximum cranial breadth	At the supramastoid crest: *N* = 12
Parietal wall sides orientation in posterior view	Slightly convergent or parallel: *N* = 13
Opisthocranium location	At the upper margin of the suprainiac surface: *N* = 8
Opisthocranium not coincident with inion	Yes: *N* = 7 Absent: *N* = 13
Parietal angular torus	Weak: *N* = 3 Strong: *N* = 1 (Cr. 4)
Temporal squama	High and very convex (arched or triangular) superior border: *N* = 12
Mastoid process	Well projecting from the surrounding occipitomastoid region: *N* = 9
Anterior mastoid tubercle	Absent: *N* = 12
Postglenoid process	Well developed: *N* = 11
Articular eminence	Flattened: *N* = 11
Tympanic plate orientation	Coronally: *N* = 10 Sagittally: *N* = 1 (Cr. 4)
Styloid process	Fused to the basicranium: *N* = 12
Styloid process position	Aligned with the stylomastoid foramen and the digastric groove: *N* = 12
Supraorbital torus shape	Continuity of the lateral, orbital and glabellar segments: *N* = 10 Change of plane between the glabellar and orbital segments: *N* = 1 (Cr. 13)
Glabellar region shape	Inflated region without a midline depression: *N* = 10 Inflated but with a midline depression: *N* = 1 (Cr. 13)
Nasal bones projection	Projecting: *N* = 5
Nasal root sagittal position	At the same level as the glabella: *N* = 7
Internal nasal rim	Absent: *N* = 7
Middle projection of the walls of the nasal cavity	Absent: *N* = 7
Infraorbital plate morphology	The infraorbital plate is not diagonally oriented as in Neanderthals, nor coronally as in modern humans; the maxilla is inflated and there is no canine fossa; the zygomaxillaryalveolar crest is straight or gently arched and the root is placed midway between the low (Neandertal) and the high (modern human) character states: *N* = 7
Maxillary torus	Present: *N* = 1 (Cr. 15; but reduced to tubercles) Absent: *N* = 5

eminence is weakly developed in the SH sample, as in Neandertals and European MPHs (*25*, *28*). These traits could be functionally related to the low position of the mandibular condyle present in SH, and in some other European MPHs and Neandertals (*29*) (see below). Thus, the anterior portion of the temporal bone (functionally related to the masticatory apparatus) shows derived Neandertal features, whereas the posterior (occipitomastoid) region remains primitive.

Mandibles and dentition

The SH mandibles also show several derived Neandertal features (*30*, *31*). The sample is morphologically consistent, although some size-related variation is present, with larger specimens generally showing more posteriorly placed structures of the lateral corpus and larger retromolar spaces than smaller individuals (fig. S9). In addition, the SH mandibles show an asymmetrical configuration of the superior margin of the ramus, with a relatively low position of the condyle, a medial insertion of the incisure crest at the condyle. and a well-developed lateral pterygoid fossa on the medial aspect of the condylar neck. This suite of ramus features has been suggested to reflect a masticatory specialization in Neandertals (*29*).

Besides these derived Neandertal features, some distinctions from the Neandertals, reflecting the retention of primitive features, are also apparent. The SH mandibles show a more retreating symphyseal angle, and wider bigonial breadth (table S2), reflecting the general absence of truncation and inversion of the gonial margin typical of Neandertals. The ramus is wider in SH and the horizontal/oval (H-O) form of the mandibular foramen is absent (except in AT-2553). Finally, on the internal aspect of the mandibular corpus, the mylohyoid line is less diagonally inclined, and the submandibular fossae are shallower for the SH hominins.

The SH dentition presents most of the morphological traits usually considered characteristic of the Neandertals (*32*). In addition, the SH hominins have some likely homoplastic features that are particular to this population and are comparable to those of modern humans but are not found in other archaic *Homo* taxa (*33*). These include absolutely small posterior teeth (*34*), similar intermolar size ratios, frequent absence of hypoconulid and hypocone, and the pattern of cusp proportions in the M^1 (*33*, *35*, *36*).

Discussion

The chronology established for LU-6 and LU-7, on the basis of several independent techniques with reproducible results, provides a minimum age of ~430 ka for the SH human fossils, which is some 100 ka younger than previously reported (*37*). With this new age, the SH hominins are now the oldest reliably dated hominins to show clear Neandertal apomorphies. Notably, the improved chronology for the SH assemblage is compatible with the latest dental and genetic evidence for Middle Pleistocene evolutionary divergences (*38*, *39*) and enables us to state with certainty that the modern human/Neandertal most recent common ancestor dates to sometime before ~430 ka (pre–MIS 11).

The considerably enlarged SH cranial sample is morphologically quite homogeneous. In addition to some plesiomorphic traits in the cranial vault (such as the low position of the maximum cranial breadth), derived Neandertal traits are present in the midfacial projection, morphology of the supraorbital torus, and the glenoid cavity. Although the occipital morphology is not Neandertal-like, there is a flat supratoral surface that may be derived in the direction of the Neandertals. Finally, the SH mandibles and the dentition also show a derived Neandertal pattern, together with some distinctive dental features. In sum, the SH sample shows a constellation of derived Neandertal facial, dental, mandibular, and glenoid features that appears to represent a single functional masticatory complex. At the same time, the cranial vault lacks Neandertal specializations. This mosaic pattern fits the prediction of the accretion model for the first stage of Neandertal evolution.

Concerning the taxonomy of the SH fossils, we have long maintained that the SH hominins are members of the Neandertal lineage (*16*, *40*). Based on the cranial evidence, we have proposed that the SH fossils, as well as the rest of the European early and middle Middle Pleistocene specimens, should be assigned to the species *Homo heidelbergensis* defined in a broad sense to include fossils with a generally more primitive morphology than the late Middle Pleistocene and Late Pleistocene Neandertals, even if they exhibit some derived Neandertal traits (*19*). However, the difficulty with identifying derived Neandertal features in the Mauer mandible, the type specimen of *H. heidelbergensis*, contrasts strongly with the presence of numerous Neandertal apomorphies in the SH mandibles (*41*). On this basis, we suggest that the SH sample be removed from the *H. heidelbergensis* hypodigm. An alternative view of *H. heidelbergensis* is as a Middle Pleistocene taxon that includes only fossils that lack any Neandertal apomorphies, and, in this restricted sense, the species is seen as the stem group for Neandertals and modern humans (*7*).

In addition, the new evidence presented here based on cranial morphology confirms that the SH population differs from some other European MPHs, such as Ceprano and Arago, that do not exhibit the suite of derived Neandertal features seen in SH. Thus, more than one evolutionary lineage appears to have coexisted during the European Middle Pleistocene (*42*), with that represented by the SH sample being phylogenetically closer (i.e., a sister group) to the Neandertals.

Some authors have, indeed, recommended that the SH fossils be included in *H. neanderthalensis* (*5*, *7*) as early members of this evolutionary lineage. However, although we agree that the SH hominins are members of the Neandertal clade, the present analysis has shown that they differ from Neandertals in several cranial regions that are considered taxonomically diagnostic of *H. neanderthalensis*. We argue that the SH p-deme is sufficiently different from that of *H. neanderthalensis* so as to be considered a separate taxon. Whether this difference should be recognized on the specific or subspecific level is currently an open question.

Related to this, a nearly complete mitochondrial genome recently sequenced from a SH femur (*43*) groups with two Denisovan individuals rather than with Neandertals. This surprising result might seem to contradict our morphological interpretation of the SH population belonging to the Neandertal clade. However, based on analysis of their nuclear genome, the Denisovans are considered a sister group to Neandertals (*44*). It is possible that two deeply divergent mitochondrial DNA (mtDNA) lineages coexisted in the SH population, one that later characterizes the Denisovans and another (as yet undocumented) mtDNA lineage that became fixed in Neandertals. Alternatively, it is possible that gene flow from another hominin population (not belonging to the Neandertal clade) brought the Denisova-like mtDNA into the SH population or its ancestors. The latter scenario would imply that two different hominin clades (the Neandertal clade and another more primitive clade) coexisted in Europe for some time, an interpretation that is not contradicted by the fossil evidence. Retrieving additional mitochondrial or nuclear DNA sequences from the SH sample may help clarify our understanding.

It is important to underline that the morphology of the SH crania, mandibles, and teeth is very constant for those features that have been considered taxonomically relevant, without polymorphisms or different trait combinations. This finding was not a foregone conclusion, because the SH variation could have encompassed the range of variation found among different European fossils that are broadly contemporaneous. However, it is clear that there is more variation between demes in the European mid Middle Pleistocene than there is within the SH deme. The morphological variability among a single p-deme can be used to distinguish between anagenetic (linear) or cladogenetic (branching) patterns of evolution. The former implies that the population as a whole (of which any particular p-deme is but one component) evolves in a similar direction throughout its geographic range, and that the individual p-demes show a large degree of intrademe morphological variation. In contrast, the latter is more consistent with the cladogenetic model and implies that evolutionary change occurs via sorting between p-demes, which individually show little intrademe variation.

Although the accretion model is potentially consistent with either an anagenetic or cladogenetic mode of evolution, our morphological analysis of the SH sample fits the latter more closely. Moreover, the scenario of several demographic crashes influenced by climatic crisis throughout the European Middle Pleistocene would produce p-deme sorting, with extinction of some populations and replacement by others (*5*). The presence in the SH skulls of Neandertal-derived regions that can be functionally related in modules, together with others that remain primitive, combined with the pre-MIS 11 age of the sample, confirms the accretion model of Neandertal origins. Finally, the finding that these derived Neandertal features are functionally related with the masticatory complex suggests that the origin of the Neandertal clade coincides with a masticatory specialization.

REFERENCES AND NOTES

1. J.-J. Hublin, *Geobios Mem. Spec.* **15**, 345–357 (1982).
2. G. P. Rightmire, *Evol. Anthropol.* **17**, 8–21 (2008).
3. C. B. Stringer, in *Ancestors: The Hard Evidence*, E. Delson, Ed. (Liss, New York, 1985), pp. 285–295.
4. J. H. Schwartz, I. Tattersall, *Am. J. Phys. Anthropol.* **143** (suppl. 51), 94–121 (2010).
5. J. J. Hublin, *Proc. Natl. Acad. Sci. U.S.A.* **106**, 16022–16027 (2009).
6. G. P. Rightmire, *Evol. Anthropol.* **6**, 218–227 (1998).
7. C. Stringer, *Evol. Anthropol.* **21**, 101–107 (2012).
8. I. Tattersall, *Proc. Natl. Acad. Sci. U.S.A.* **106**, 16018–16021 (2009).
9. M. H. Wolpoff, in *The Human Revolution: Behavioural and Biological Perspectives in the Origins of Modern Humans*, P. Mellars, C. Stringer, Eds. (Edinburgh Univ. Press, Edinburgh, 1989), pp. 62–108.
10. D. Dean, J. J. Hublin, R. Holloway, R. Ziegler, *J. Hum. Evol.* **34**, 485–508 (1998).
11. C. B. Stringer, J. Hublin, *J. Hum. Evol.* **37**, 873–877 (1999).
12. Supplementary materials are available on *Science* Online.
13. J. L. Arsuaga *et al.*, *J. Hum. Evol.* **33**, 109–127 (1997).
14. J. M. Parés, A. Pérez-González, A. B. Weil, J. L. Arsuaga, *Am. J. Phys. Anthropol.* **111**, 451–461 (2000).
15. J. L. Arsuaga, I. Martínez, A. Gracia, *Anthropologie* **105**, 161–178 (2001).
16. J. L. Arsuaga, I. Martínez, A. Gracia, J. M. Carretero, E. Carbonell, *Nature* **362**, 534–537 (1993).
17. P. Andrews, *Cour. Forsch. Inst. Senckenberg* **69**, 167–175 (1984).
18. B. A. Wood, *Cour. Forsch. Inst. Senckenberg* **69**, 99–111 (1984).
19. J. L. Arsuaga, I. Martínez, A. Gracia, C. Lorenzo, *J. Hum. Evol.* **33**, 219–281 (1997).
20. J. J. Hublin, *C. R. Acad. Sci. Paris Ser. D* **287**, 923-926 (1978).
21. C. B. Stringer, J. J. Hublin, B. Vandermeersch, in *The Origin of Modern Humans: A World Survey of the Fossil Evidence*, F. H. Smith, F. Spencer, Eds. (Liss, New York, 1984), pp. 51–135.
22. J. H. Schwartz, I. Tattersall, *Proc. Natl. Acad. Sci. U.S.A.* **93**, 10852–10854 (1996).
23. J. H. Schwartz, I. Tattersall, M. Teschler-Nicola, *Anat. Rec.* **291**, 1517–1534 (2008).
24. R. G. Franciscus, *J. Hum. Evol.* **44**, 701–729 (2003).
25. I. Martínez, J. L. Arsuaga, *J. Hum. Evol.* **33**, 283–318 (1997).
26. M. Elyatqine, thesis, Université Bordeaux I, France (1995).
27. S. Condemi, in *L'Homme de Neandertal*, E. Trinkaus, Ed. (Etudes et Recherche Archéologiques de l'Université de Liége, Liège, France), 1988), vol. 3, pp. 49–53.
28. I. Martínez, R. Quam, J. L. Arsuaga, *Period. Biol.* **108**, 309–317 (2006).
29. Y. Rak, A. Ginzburg, E. Geffen, *Am. J. Phys. Anthropol.* **119**, 199–204 (2002).
30. J. Daura *et al.*, *J. Hum. Evol.* **49**, 56–70 (2005).
31. A. Rosas, *Am. J. Phys. Anthropol.* **114**, 74–91 (2001).
32. M. Martinón-Torres, J. M. Bermúdez de Castro, A. Gómez-Robles, L. Prado-Simón, J. L. Arsuaga, *J. Hum. Evol.* **62**, 7–58 (2012).
33. M. Martinón-Torres *et al.*, *J. Anat.* **223**, 353–363 (2013).
34. J. M. Bermúdez de Castro, *J. Hum. Evol.* **15**, 265–287 (1986).
35. J. M. Bermúdez de Castro, M. E. Nicolas, *Am. J. Phys. Anthropol.* **96**, 335–356 (1995).
36. A. Gómez-Robles, J. M. Bermúdez de Castro, M. Martinón-Torres, L. Prado-Simón, J. L. Arsuaga, *J. Hum. Evol.* **63**, 512–526 (2012).
37. J. L. Bischoff *et al.*, *J. Archaeol. Sci.* **34**, 763–770 (2007).
38. P. Endicott, S. Y. W. Ho, C. Stringer, *J. Hum. Evol.* **59**, 87–95 (2010).
39. A. Gómez-Robles, J. M. Bermúdez de Castro, J.-L. Arsuaga, E. Carbonell, P. D. Polly, *Proc. Natl. Acad. Sci. U.S.A.* **110**, 18196–18201 (2013).
40. J. L. Arsuaga, J. M. Carretero, I. Martínez, A. Gracia, *J. Hum. Evol.* **20**, 191–230 (1991).

41. Y. Rak *et al.*, *Am. J. Phys. Anthropol.* **144**, 247 (2011).
42. I. Tattersall, in *Continuity and Discontinuity in the Peopling of Europe: One Hundred Fifty Years of Neanderthal Study*, S. Condemi, G.-C. Weniger, Eds. (Springer Science+Business Media B.V., New York, 2011), chap. 4.
43. M. Meyer *et al.*, *Nature* **505**, 403–406 (2014).
44. M. Meyer *et al.*, *Science* **338**, 222–226 (2012).
45. L. J. Arnold *et al.*, *J. Hum. Evol.* **67**, 85–107 (2014).

ACKNOWLEDGMENTS

We are grateful to the Atapuerca team, especially A. Esquivel for work in SH and M. C. Ortega for restoration of the SH fossils, and to K. Ludwig, J. Rofes, and J. M. López-García for constructive discussions. E. Santos assisted with computed tomography scanning and J. Trueba provided the photos. For access to the comparative materials, we thank P. Mennecier, A. Froment, H. de Lumley, D. Grimaud-Hervé, C. B. Stringer, R. Kruszynski, G. D. Koufous, D. Mania, D. Lieberman, and J. Haas. A.G.-T. has a contract from the Ramón y Cajal Program (RYC-2010-06152). R.M.Q. received financial support from BU-SUNY and the AMNH. A.P.-P. has a MECD grant (AP-2009-4096). E.P.-R. has a CAM grant (S2010/BMD-2330). A.A.V. has a MINECO grant (BES-2010-039961). A.G.-O. and M.D. have a Marie Curie–IEF and a Marie Curie–IRG (PIRG8-GA-2010-276810) contracts. N.S., A.B., L.R., A.P.-P., A.A.V., and R.G. received Fundación Atapuerca grants. L.J.A. has an ARCFF grant (FT130100195). Dating at the Berkeley Geochronology Center was supported by the Ann and Gordon Getty Foundation. U-Th isotopic analysis at the HISPEC was supported by Taiwan ROC MOST and NTU grants (100-2116-M-002-009, 101-2116-M-002-009, 101R7625). Thanks to SGIker-UPV/EHU for their research facilities. This research was supported by the MINECO (CGL2012-38434-C03-01 and 03) and the JCyL (BU005A09, DGR 2009 SGR-324) projects. Fieldwork was funded by the JCyL and the Fundación Atapuerca. Junta de Castilla y León is the repository of the fossils.

SUPPLEMENTARY MATERIALS

www.sciencemag.org/content/344/6190/1358/suppl/DC1
Materials and Methods
Supplementary Text S1 to S9
Figs. S1 to S39
Tables S1 to S15
References (*46*–*178*)

26 March 2014; accepted 12 May 2014
10.1126/science.1253958

REPORTS

QUANTUM MECHANICS

An electronic quantum eraser

E. Weisz,* H. K. Choi,* I. Sivan, M. Heiblum,† Y. Gefen, D. Mahalu, V. Umansky

The quantum eraser is a device that illustrates the quantum principle of complementarity and shows how a dephased system can regain its lost quantum behavior by erasing the "which-path" information already obtained about it. Thus far, quantum erasers were constructed predominantly in optical systems. Here, we present a realization of a quantum eraser in a mesoscopic electronic device. The use of interacting electrons, instead of noninteracting photons, allows control over the extracted information and a smooth variation of the degree of quantum erasure. The demonstrated system can serve as a first step toward a variety of more complex setups.

Complementarity in quantum measurements is a core concept of quantum mechanics (*1*), closely related to Heisenberg's uncertainty principle, although the exact relation between the two remains a source of debate (*2*–*8*). An example of complementarity is the double-slit interference experiment: If we measure a particle's position, the measurement will quench its wavelike nature; vice versa, observing the wave behavior via interference implies lack of knowledge of the particle's path. A canonical system for exploring complementarity is the quantum eraser, predominantly studied in photonic systems (*9*–*16*). A quantum eraser is an interference experiment consisting of two stages. First, one of the interfering paths is coupled to a "which-path" detector, resulting in loss of interference due to acquisition of which-path information. Second, the which-path information is being "erased" by projecting the detector's wave function on an adequately chosen basis; this renders the which-path information inaccessible, which allows reconstruction of the interference pattern.

Here, we present an implementation of a quantum eraser in an electronic system. Our system consists of two identical electronic Mach-Zehnder interferometers (MZIs) (*17*) entangled via Coulomb interactions. Initially proposed by Kang (*18*) and studied theoretically in (*19*, *20*), this setup consists of two MZI: one serving as a path detector and the other as the system interferometer, where the visibility of the Aharonov-Bohm (AB) oscillation in the system can be controlled by the detector (*21*–*23*).

An electronic MZI is formed by manipulating quasi–one-dimensional, chiral edge channels, which are formed in the integer quantum Hall effect regime (*17*). Potential barriers, formed by quantum point contacts (QPCs), take the role of optical beam splitters, transmitting and reflecting impinging electrons with amplitudes t_i and r_i, respectively, where $|t_i|^2 + |r_i|^2 = 1$ and $t_i, r_i \in R$. Two such coupled MZIs are shown in Fig. 1, where the coupling is mediated by the lower path of the system and the upper path of the detector, referred to as interacting paths (shaded area in Fig. 1A).

Starting with the system, an electron injected from source S1 arrives at SQPC1 and is put into a superposition of being reflected into the interacting path and transmitted into the noninteracting path, namely, $|S\rangle = r_1|\uparrow\rangle_S + t_1|\downarrow\rangle_S$, with $|\uparrow\rangle_S$ and $|\downarrow\rangle_S$ standing for the interacting and noninteracting paths of the system, respectively. The paths recombine and interfere at SQPC2, with the electron's probability of reaching the drain D2 being $P(\mathrm{D2}) = |r_1 r_2 e^{i\phi_S} - t_1 t_2|^2 = T_0 - T_1\cos(\phi_S)$, where $T_0 \equiv |t_1 t_2|^2 + |r_1 r_2|^2$, $T_1 \equiv 2t_1 t_2 r_1 r_2$, $\phi_S = 2\pi AB/\Phi_0$ is the AB phase (*24*), $\Phi_0 = h/e$ is the magnetic flux quantum, A the area enclosed by the two paths, and B the magnetic field. The visibility of the interfering pattern at D2 is defined as $v_{\mathrm{D2}} \equiv \frac{\max[P(\mathrm{D2})] - \min[P(\mathrm{D2})]}{\max[P(\mathrm{D2})] + \min[P(\mathrm{D2})]} = \frac{T_1}{T_0}$. Throughout our experiments, all the QPCs were tuned to have equal transmission and reflection amplitudes, $|r_i|^2 = |t_i|^2 = \frac{1}{2}$; $i = 1...4$.

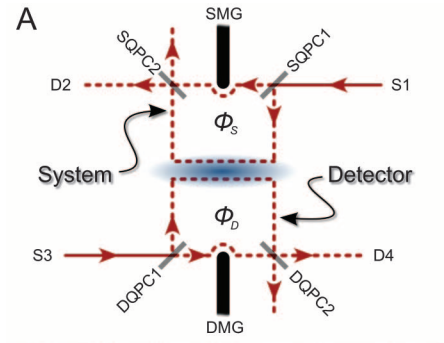

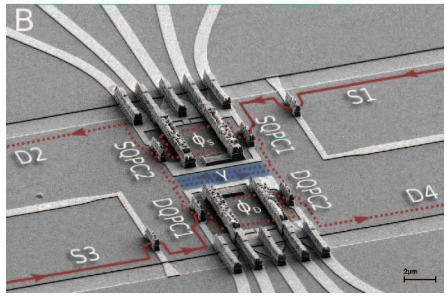

Fig. 1. Schematics and micrograph of the device under study. (**A**) The electronic quantum eraser consists of two identical electronic Mach-Zehnder interferometers (MZIs) entangled via Coulomb interactions. Quantum point contacts (QPCs) serve as beam splitters (full lines represent full beams, and dashed lines partitioned beams). (**B**) A scanning electron microscope micrograph of the fabricated structure, which was realized in a GaAs-AlGaAs heterostructure harboring a high-mobility two-dimensional electron gas. The edge channels were manipulated by biasing surface gates (bright gray) and surface etching. Ohmic contacts serve as sources (S1, S3) and drains (D2, D4), which allow electric access to the electron gas lying underneath the surface. The nanostructures were defined using electron-beam lithography.

Braun Center for Submicron Research, Department of Condensed Matter Physics, Weizmann Institute of Science, Rehovot 76100, Israel.
*These authors contributed equally to this work. **†Corresponding author. E-mail: moty.heiblum@weizmann.ac.il**